

On the zirconium oxide neutral cluster distribution in the gas phase: Detection through 118 nm single photon, and 193 and 355 nm multiphoton, ionization

Y. Matsuda, D. N. Shin, and E. R. Bernstein

Citation: *The Journal of Chemical Physics* **120**, 4142 (2004); doi: 10.1063/1.1643731

View online: <http://dx.doi.org/10.1063/1.1643731>

View Table of Contents: <http://aip.scitation.org/toc/jcp/120/9>

Published by the [American Institute of Physics](#)

COMPLETELY

REDESIGNED!



**PHYSICS
TODAY**

Physics Today Buyer's Guide
Search with a purpose.

On the zirconium oxide neutral cluster distribution in the gas phase: Detection through 118 nm single photon, and 193 and 355 nm multiphoton, ionization

Y. Matsuda, D. N. Shin, and E. R. Bernstein

Department of Chemistry, Colorado State University, Fort Collins, Colorado 80523-1872

(Received 5 September 2003; accepted 2 December 2003)

Zirconium oxide clusters are generated in the gas phase by laser ablation of the metal into a flow of ca. 5% O₂/95% He at 100 psig and supersonic expansion into a vacuum chamber. Mass spectra of neutral gas phase zirconium oxide clusters are obtained through photoionization at three different laser wavelengths: 118, 193, and 355 nm. Ionization of the clusters with 118 nm laser radiation is through a single photon ionization mechanism, while ionization by 193 and 355 nm laser radiation is through a multiphoton (three or more photon) mechanism. Fragment ion features are observed in the mass spectra of Zr_mO_n⁺ for only the 193 nm and 355 nm ionization schemes. The true neutral Zr_mO_n cluster distribution is obtained only through 118 nm single photon ionization, as verified by mass spectral peak linewidths and calculations of the cluster binding energies, ionization energies, and fragmentation rates. The neutral cluster distribution consists mainly of the series Zr_mO_{2m} and Zr_mO_{2m+1} for m = 1, ..., ~30. © 2004 American Institute of Physics. [DOI: 10.1063/1.1643731]

I. INTRODUCTION

Transition metal oxides are an important series of practical heterogeneous catalysts and their properties and reactions have been extensively studied.^{1–5} Nonetheless, uncovering the detailed, microscopic geometrical and electronic structure of an active catalytic site, and thereby generating a reaction mechanism for a heterogeneous catalytic reaction, is still an elusive goal.

Neutral metal oxide clusters have a wide variety of electronic and structural properties that in some instances reflect bulk properties and in others reflect defect or surface structures.^{6–10} Various sizes of metal oxide clusters can be produced and/or emphasized^{11–19} that have their own specific characteristics (cluster structure, bond energy, ionization threshold, electronic states) and even reactivities (V_mO_n, Zr_mO_n, Fe_mO_n, Cu_mO_n).^{11–13} Metal oxide cluster properties, structures, reactivities, and catalytic efficacy should change with cluster size. One can anticipate that a particular cluster or subset of clusters will possess properties that resemble those of surface or bulk materials that are catalytically active. Clusters are, however, much easier and simpler to study in detail, both experimentally and theoretically, than are surfaces or bulk materials with defects.¹⁴ Therefore, systematic exploration of the properties, reactions, and catalytic reactivities of neutral transition metal oxide clusters as a function of cluster size should generate a fundamental understanding of the practical application of metal oxide species in catalysis.

Numerous studies of anionic, neutral, and cationic metal oxide clusters have been performed in recent years employing UV and IR multiphoton ionization mass spectroscopy, photoelectron spectroscopy, and microwave spectroscopy.^{15–21} Electronic spectroscopy of metal oxide clusters has been limited to small (diatomic and triatomic) clusters

because of the large density of electronic states that most M_mO_n species have. Elucidation of the neutral cluster distribution and knowledge of the thermodynamically stable species in the gas phase can generate information on cluster nucleation and growth mechanisms and stable neutral cluster structures. Mass spectra representing the neutral cluster distribution are thus a first step in the understanding of neutral metal oxide clusters.

The neutral metal oxide cluster distribution in the gas phase can be determined by mass spectroscopy; however, the clusters must first be ionized to be detected. One of the most gentle and precise methods of cluster ionization is by a photon, but metal oxide clusters typically have ionization energies greater than 6.5 eV; single photon ionization is thus difficult but not impossible to achieve.¹³ Typically the neutral cluster distribution is ionized by multiphoton ionization processes at 193 nm (ArF laser) during which from 2 to 10 or more photons can be absorbed by the M_xO_y clusters due to their high density of electronic states for both neutral and cationic species. Under these conditions, cluster fragmentation is typical¹² and subsequent loss of M, O, M_a, O_b, M_xO_y, etc., species compromises the attempt to observe the neutral cluster distribution through mass spectroscopic techniques.

Recently, 118 nm radiation, generated from the ninth harmonic of a Nd/YAG laser (1064 nm) fundamental output (1064 nm–KDP–355 nm–Xe/Ar–118 nm), has been applied to ionize several cluster systems [e.g., C_n,²² (CH₃OH)_n,²³ (CH₃CH₂OH)_n,²³ Fe_mO_n,¹³ Cu_mO_n,¹³ Ti_mO_n,¹³ V_mO_n,¹³ (Ref. 13)] by a single photon mechanism. Kaizic *et al.*²¹ report mass spectra of neutral carbon clusters detected through 118 nm laser ionization that are quite different from those ionized through a multiphoton technique. Metal oxide clusters can be expected to ionize by a single photon mechanism employing 118 nm (10.5 eV) radiation, and thus these clus-

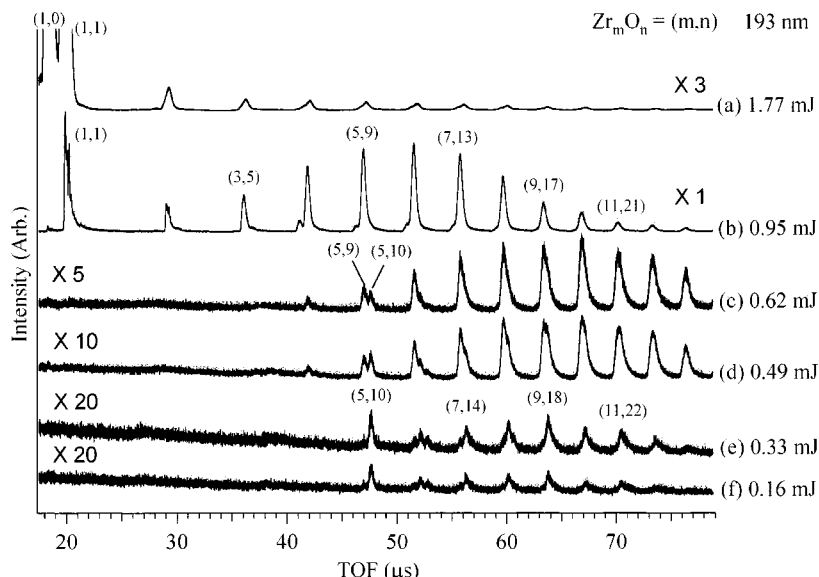


FIG. 1. TOF mass spectra of zirconium oxide clusters measured by 193 nm laser ionization with different energies/pulse as indicated.

ters will not in general be fragmented in the detection process.

The neutral cluster distribution for zirconium oxide has been studied in the last few years by two multiphoton ionization techniques. Foltin *et al.*¹² report mass spectra of Zr_mO_n species using 193 nm laser ionization. In intense 193 nm laser light, only $Zr_mO_{m-1}^+$ species are observed and the approach of covariance mapping of the mass spectral features supports the mechanism of multiphoton ionization/neutral cluster fragmentation for the detection process. If the ionization laser intensity for 193 nm is greatly reduced, only clusters of the form Zr_mO_{2m} ($m \geq 5$) are observed and the Zr_mO_{2m-1} series disappears. van Holden *et al.*¹⁵ use high fluence IR radiation to ionize Zr_mO_n clusters by a multiphoton process and again only $Zr_mO_{2m-1}^+$ clusters are detected with an intensity pattern that is similar to that observed by UV (193 nm) multiphoton ionization. In general one can conclude that multiphoton ionization (more than three photons at 193 nm and more than 30 photons at ca. 1000 cm^{-1}) leads to neutral cluster fragmentation for the Zr_mO_n clusters system.

In the present study of the neutral cluster distribution of Zr_mO_n species (created by laser ablation of the metal into an O_2/He mixture, which then undergoes a supersonic expansion into a vacuum system), both single photon (118 nm) and multiphoton (193 and 355 nm) ionization techniques are employed. For the multiphoton ionization processes, only $Zr_mO_{2m-1}^+$ species are observed. For the single photon ionization processes, the most intense series of clusters are of the forms $Zr_mO_{2m}^+$ and $Zr_mO_{2m+1}^+$ and the cluster series $Zr_mO_{2m-1}^+$ is not observed.

Mass spectral features are analyzed for both single and multiphoton ionization processes: ions created by multiphoton processes (193 and 355 nm radiation) have mass spectral peak linewidths greater than 20 ns, while ion peaks created by single photon processes (118 nm radiation) have linewidths ca. 10 ns reflecting the laser pulsewidth. Based on linewidth data and calculations of cluster ionization energies, bonding energies, and fragmentation probabilities, we con-

clude that the thermodynamically stable neutral clusters are of the forms Zr_mO_{2m} and Zr_mO_{2m+1} .

II. EXPERIMENTAL PROCEDURES

The experimental procedures and apparatus employed in these studies are similar to those described in Refs. 11–13. Briefly, the Zr_mO_n clusters are generated by laser ablation of the metal into a gas mixture of 6% $O_2/94\%$ He. This mixture of helium gas and Zr_mO_n is then expanded into a vacuum system through a 2 mm \times 5 cm nozzle channel. The backing pressure of the expansion/reaction gas mixture is 100 psig. The pulsed supersonic nozzle/laser ablation/cluster source is most recently described in Ref. 12. The Zr metal foil (0.1 mm thick, 99.98% pure) for ablation is purchased from Aldrich Chemical Co.

The generated clusters pass through a skimmer and into a time-of-flight mass spectrometer (TOFMS, Wiley-McLaren design) where they are ionized by laser (355, 193, 118 nm) radiation.¹³ The experimental timing is controlled by an SRS DG535 time delay/pulse generator (Stanford Research Systems) and the microchannel plate detector output is captured and stored (pulse by pulse, at a 10 Hz rate) by a RTD 720A (Tektronix) transient digitizer connected to a personal computer. In order to ensure accurate timing for ion arrival and detection times, a photodiode monitoring the ionization laser pulse is employed to generate a zero of time. This zero time point removes fluctuations associated with the laser firing. A true time zero for each spectrum is obtained from this diode pulse and from fitting mass peaks. The accuracy or residual error for this procedure is 1 ns or less.

III. RESULTS

Figure 1 shows the TOFMS of Zr_mO_n clusters collected by 193 nm radiation ionization. Spectra (b) and (e) of this figure are essentially the same as those reported by Ref. 12. In spectrum (b), a series of mass spectral peaks of the form $Zr_mO_{2m-1}^+$ are the main features. The mass spectrum of Zr_mO_n clusters measured with IR (1000 cm^{-1}) multiphoton

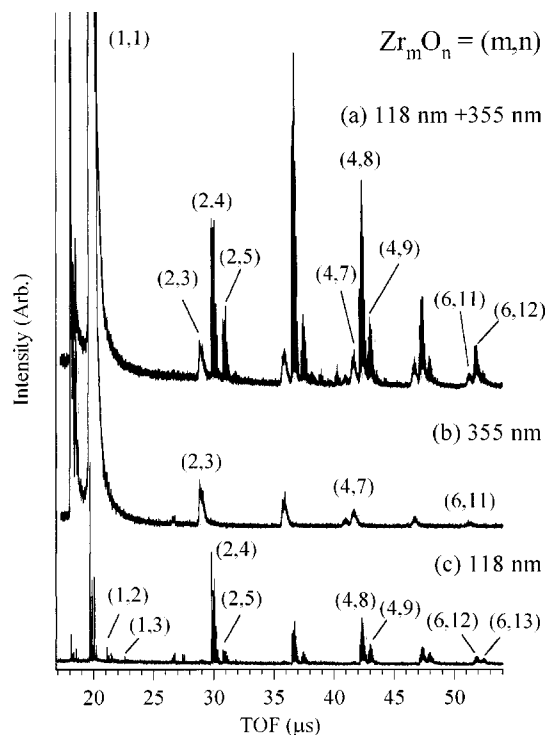


FIG. 2. TOF mass spectra of zirconium oxide clusters that are ionized by (a) 118 nm and 355 nm (24 mJ/pulse), (b) 355 nm (24 mJ/pulse), and (c) 118 nm (17 mJ/pulse at 355 nm).

laser ionization¹⁵ shows essentially the same features and relative intensities. The peak intensities of the $Zr_mO_{2m-1}^+$ ($m > 2$) are decreased with higher 193 nm laser energy/pulse (> 1 mJ/pulse) as shown in Fig. 1(a). This decrease of peak intensity for $m > 2$ results in an increase in the Zr and ZrO intensities as can be seen in Fig. 1(a) compared to Fig. 1(b). On the other hand, if the laser intensity is reduced to ca. 0.6 mJ/pulse at 193 nm, the mass spectrum begins to change and features belonging to series $Zr_mO_{2m}^+$ appear for $m \geq 5$. As the ionization laser energy/pulse is reduced below 0.5 mJ/pulse, the $Zr_mO_{2m}^+$ features dominate the mass spectra [see Figs. 1(c), 1(d), 1(e), and 1(f)]. These results imply that the observed $Zr_mO_{2m-1}^+$ mass spectral features arise from the fragmentation of Zr_mO_{2m} neutral clusters due to the multiphoton absorption of 193 nm photons. As the laser intensity is lowered, the $Zr_5O_{10}^+$ feature becomes the most intense peak in the spectrum. Note that with ionization laser energy/pulse below 0.5 mJ/pulse, no cluster with $m < 5$ is observed. Based on similar results, Foltin *et al.*¹² considered the Zr_5O_{10} neutral cluster to be an especially stable structure in the neutral cluster distribution.

The TOFMS measured by 118 nm and 355 nm laser ionization are shown in Fig. 2. One can easily separate the 118 nm detected mass spectrum from that detected by 355 nm ionization by comparison of the three spectra presented in this figure. The 118 nm light is generated by tripling the 355 nm light in a Xe/Ar (1:10) cell of ca. 200 torr total gas pressure.¹³ Both laser beams are transmitted to the TOFMS ionization region by the final MgF₂ lens at the cell output. The 118 nm light is focused to less than ca. 50 μm, while the 355 nm light is defocused to ca. 5 mm. The 355 nm light is

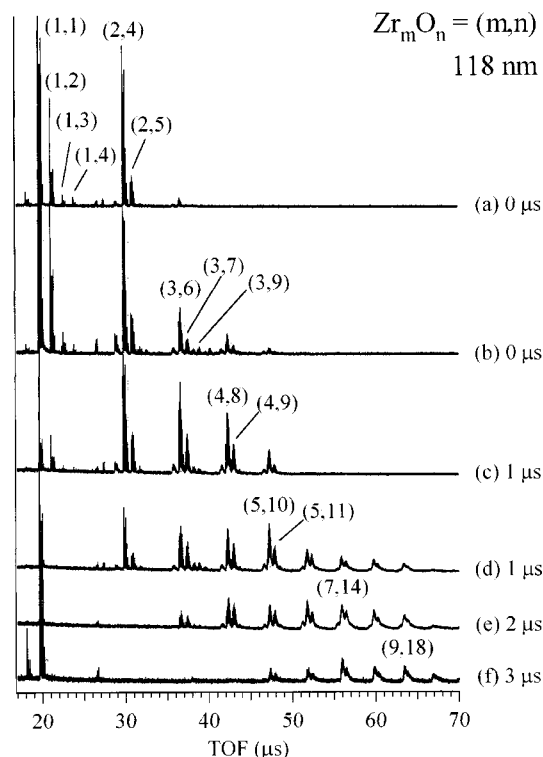


FIG. 3. TOF mass spectra of zirconium oxide clusters detected by 118 nm ionization. These spectra are measured by ionizing different regions of supersonic jet gas pulse of zirconium oxide clusters by displacing the laser horizontally a few mm and by delaying the ionization laser pulse with respect to the ablation process a few μs.

still intense enough at 23.5 mJ/pulse to generate ions by a multiphoton process. Spectrum 2(b) is generated from an evacuated tripling cell and shows a typical fragmentation, multiphoton ionization set of features. The Zr_mO_{2m-1} features in Figs. 2(a) and 2(b) have roughly the same intensity, which further suggests that they arise only from 355 nm ionization/fragmentation processes. Note also that the Zr and ZrO features are intense in these spectra due to fragmentation [compare to Figs. 2(c) and 1(a)]. In spectrum 2(a), the most intense features are of the two series Zr_mO_{2m} and Zr_mO_{2m+1} and some weaker features belonging to the series Zr_mO_n ($n > 2m + 1$) are observed. Spectrum 2(c) is obtained with 17 mJ/pulse 355 nm light [rather than 23.5 mJ/pulse for 2(a) and 2(b)] defocused to ca. 8 mm in the ionization region, and 500 torr of Xe/Ar in the cell: the Zr_mO_{2m-1} series is completely missing. This demonstrates (qualitatively) that the 355 nm ionization/fragmentation processes require more than three photons. Note that ZrO_2^+ and ZrO_3^+ peaks are observed in Fig. 2(c) and that the fragmentation features Zr^+ and ZrO^+ are very weak in this spectrum. ZrO_2^+ and ZrO_3^+ are not observed in Figs. 2(a) and 2(b) and are fragmented by the higher photon density of the 355 nm ionization beam.

Figure 3 shows the TOF mass spectra of Zr_mO_n obtained with 118 nm ionization taken as a function of timing delay between ablation and ionization laser pulses and small, ca. 1 nm translations of the interaction point between the cluster beam and ionization laser beam along the cluster beam (horizontal) axis. Larger clusters are detected by shifting the ionization laser/molecular beam intersection to later parts of the

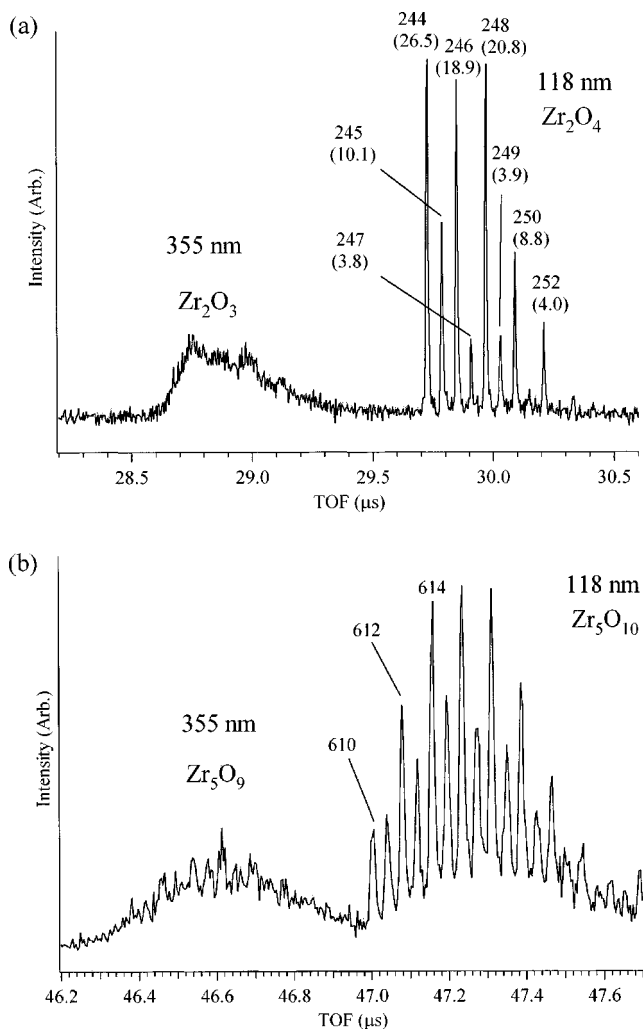


FIG. 4. Expanded TOF mass spectra of zirconium oxide clusters for (a) $Zr_2O_3^+$ and $Zr_2O_4^+$, and (b) $Zr_5O_9^+$ and $Zr_5O_{10}^+$. These spectra are measured by 118 nm and 355 nm ionization simultaneously. Peaks for $Zr_2O_4^+$ are assigned to specific isotopic masses, as are some of those for $Zr_5O_{10}^+$. The numbers in parentheses are percentages of natural abundance $Zr_2O_4^+$ estimated by abundance of zirconium isotopes. Isotopic species with less than 1% abundance are ignored. The $Zr_5O_{10}^+$ species are indicated by a few mass numbers. The $Zr_2O_4^+$ and $Zr_5O_{10}^+$ feature FWHM are both ca. 10 ns.

pulsed supersonic expansion (1 mm is equivalent to $\sim 1 \mu s$) or by delaying the ionization laser timing. Thus, the cluster size distribution is not equal throughout the gas pulse and varies considerably and systematically within the pulse due to velocity slippage [larger clusters are more slow to accelerate to beam velocity ($\sim 2 \times 10^5$ cm/s, for a He beam), and perhaps also due to time needed for larger cluster synthesis. Nonetheless, the main series of observed clusters are still Zr_mO_{2m} and Zr_mO_{2m+1} with smaller clusters having the larger concentrations. This latter fact is most likely a function of a statistical, collisional growth process. Note that this correct behavior is contrary to that observed for 193 nm ionization (even at low laser power). We will discuss this observation in the next section.

Figure 4 gives an expanded view of some of the mass spectra of Fig. 2(a). Figures 1 and 2 make the point that ionization of Zr_mO_n clusters by 193 and 355 nm radiation causes extensive cluster fragmentation. Figure 4(a) presents

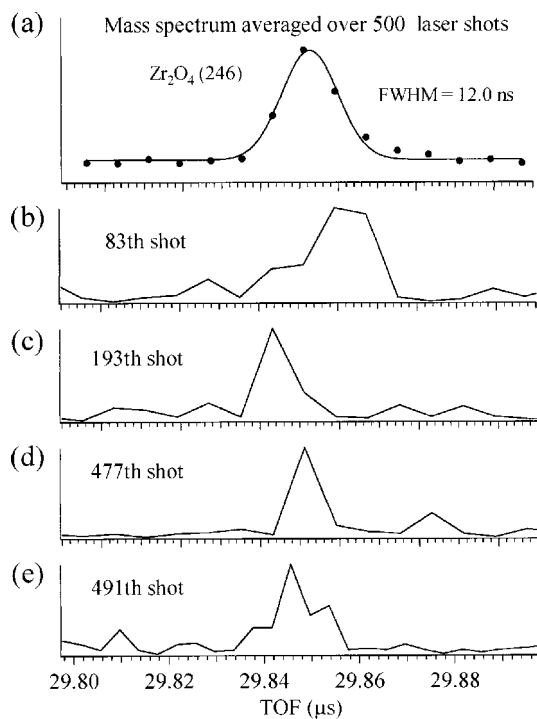


FIG. 5. (a) Expanded mass peak of $Zr_2O_4^+$ (mass 246) for a 500 shot averaged TOF mass spectra, ionized by 118 nm laser radiation. The FWHM of mass peaks, obtained by fitting the spectra to Gaussian functions is 12 ns. (b)–(e) Sample mass peaks of $Zr_2O_4^+$ (mass 246) in the single laser pulse TOF mass spectra that are averaged to generate spectrum (a). These features are roughly 2 ns FWHM, their width is limited by the transient digitizer resolution (0.25 G samples/s in these traces).

the mass spectral features $Zr_2O_3^+$ and $Zr_2O_4^+$. The numbers for the $Zr_2O_4^+$ features are isotope masses and peak intensities (in parentheses) showing the expected distribution of cluster features for two Zr atoms in the cluster (90, 91, 92, 94—ca. 5:1:1.5:1.5 natural abundance). The discrepancy between the anticipated isotopic feature intensities and those measured is probably attributable to system response time, as these spectra are obtained at 250 M samples/s for the digitizer, and the single pulse spectra can saturate the digitizer range for multiple ion events. Linewidths for the $Zr_2O_4^+$ features are ca. 10 ns and reflect the temporal laser linewidth. The width of the $Zr_2O_3^+$ feature is ca. 500 μs and reflects a distribution of decay times for the parent ions along with the now unresolved isotopic distribution. In the next section, we will discuss the implications of these results for the fragmentation mechanism. The $Zr_5O_9^+/Zr_5O_{10}^+$ spectra presented in Fig. 4(b) demonstrate similar linewidth and fragmentation behavior. Figure 5(a) shows an expanded view of one of the $Zr_2O_4^+$ mass spectral isotopic features.

The spectra presented in Fig. 5 compare the time averaged (500 laser pulses) linewidth for one of the $Zr_2O_4^+$ isotope peaks (246) and single laser pulse derived spectra of the same feature. The linewidth for a single pulse peak is smaller (< 4 ns) than the averaged one, and its peak position is slightly shifted from the average center of all 500 laser pulses which has very nearly a Gaussian line shape. These single pulse/averaged pulse differences are due to the nature of the unseeded (in this instance) Nd/YAG 1064 nm output

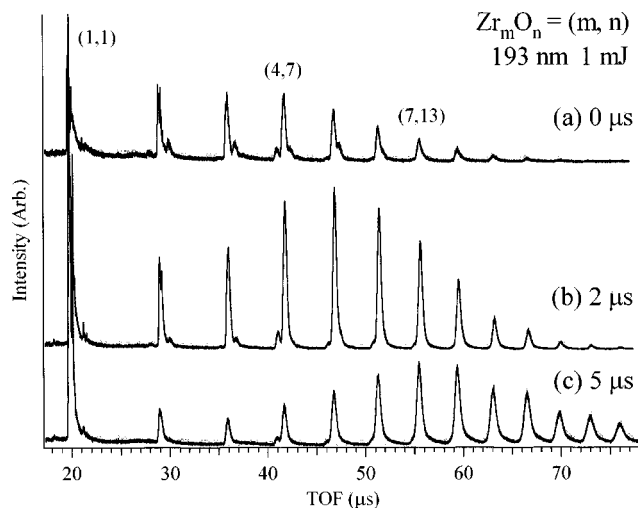


FIG. 6. TOF mass spectra of zirconium oxide clusters measured by different 193 nm ionization laser timing (b) 2 μ s and (c) 5 μ s delayed timing from spectrum (a).

pulse shape and the slight difference in the neutral cluster arrival time for each ionization laser pulse. The laser pulse is naturally somewhat mode locked with much of the output intensity coming in a few hundred ps pulses randomly distributed within the “10 ns pulse envelope.” One calculates that, for a detector gain of ca. 10^7 , a single ion creates a ca. 10 mV voltage pulse into 50 Ω . Most laser pulses produce single ion signals for each isotopic peak, as can be seen in Fig. 5. These features can be observed for two reasons: (1) the data are collected such that the detector output is separately stored for each laser pulse (at 10 Hz) and averaged only after all the 500 spectra are acquired,^{11,12} and (2) the 118 nm laser beam is tightly focused ($\leq 50 \mu$ m) so that the nonfragmented ions are all created at the same time (within the 10 ns average pulse envelope) and position in the ionization region of the TOFMS. The linewidth for the individual laser pulses is controlled by the sampling rate of the RTD720A transient digitizer (2 G sample/s but in Fig. 5 0.25 G sample/s is used). Thus, even the averaged ca. 10 ns Gaussian full width at half maximum (FWHM) of the nonfragmented mass features is composed of a distribution of narrower (ca. 2 ns) individual peaks generated by each laser pulse.

Mass spectra for $Zr_m O_n$ clusters, ionized by 1 mJ/pulse 193 nm radiation, are shown in Fig. 6 as a function of ionization laser timing. These spectra should be compared to those in Fig. 3 obtained with 118 nm ionization, also as a function of laser timing. Note that, for 118 nm ionization, the overall cluster distribution as a function of laser timing is different from that for 193 nm laser timing, even taking into account that at 193 nm detection $Zr_m O_{2m-1}^+$ clusters are observed and that at 118 nm detection, $Zr_m O_{2m,2m+1}^+$ clusters are observed. These issues will be discussed in the next section.

The low energy, 193 nm radiation detected cluster ion distribution is present in Fig. 7 as a function of ionization laser timing with respect to the ablation laser. Note that the $Zr_5 O_{10}^+$ cluster is intense under these ionization conditions for

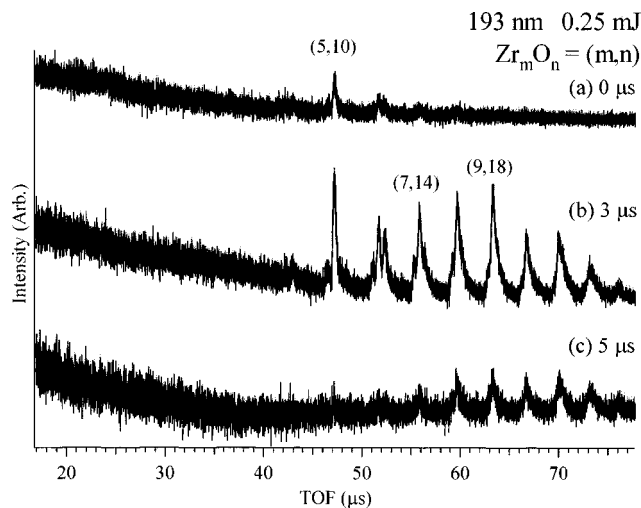


FIG. 7. TOF mass spectra of zirconium oxide clusters measured by different 193 nm ionization (0.25 mJ/pulse) laser timings; (b) 3 μ s and (c) 5 μ s delayed timing from spectrum (a).

an appropriate timing range of the ionization laser pulse. Obviously, the cluster beam is not homogeneous, but still under these conditions, the $Zr_5 O_{10}$ neutral cluster is present at high relative concentration for $m \geq 5$ (compare with spectra of Fig. 3).

IV. DISCUSSION

In this section we will discuss two related topics: (1) the gas phase neutral cluster distribution for zirconium oxide clusters generated by laser ablation of the metal, reaction of the metal atoms, clusters, and ions with oxygen, and subsequent cooling (perhaps growth) of the reaction products by supersonic expansion into a vacuum (ca. 100 psig to ca. 5×10^{-6} torr); and (2) fragmentation mechanisms for neutral clusters upon ionization by 193 and 355 nm radiation.

A. The neutral cluster distribution

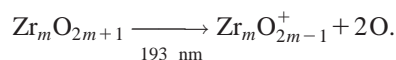
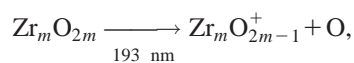
All of the data reported in this paper (linewidths, ionization intensity patterns, timing) support the conclusion that the 118 nm ionization results represent the true neutral cluster distribution; that is, the most stable, neutral clusters are of the forms $Zr_m O_{2m}$ and $Zr_m O_{2m+1}$, for $m = 1, \dots, < 30$. ZrO and ZrO_3 clusters are also present, along with the less abundant series $Zr_m O_{2m+2,3,4}$. These latter cluster series and ZrO_3 are not observed if the mass distribution is detected through 355 or 193 nm ionization. Thus, 118 nm ionization does not fragment the neutral cluster distribution. This conclusion is further supported by RRK and density functional theory (DFT) calculations discussed below in the context of a fragmentation mechanism.

An estimate of the relative abundances of the neutral clusters within each of these series ($Zr_m O_{2m}$ and $Zr_m O_{2m+1}$) and between series can be obtained from Fig. 3. Clearly the most abundant (intense signal) clusters are the small ones, ZrO , ZrO_2 , $Zr_2 O_{4,5}, \dots$. Using 10.5 eV radiation for ionization should avoid problems with small clusters having a higher ionization energy than larger ones (see below for calculations and Figs. 1 and 7 for 193 nm, low intensity ioniza-

tion mass spectra). This distribution, with abundant small and fewer large clusters, is typical of a statistical growth dominated cluster system.^{11,12} Within this general trend, cluster Zr_5O_{10} and ca. Zr_7O_{14} to Zr_9O_{18} seem to be somewhat more abundant than their immediate neighbors in the neutral cluster distribution. Note that this is not a simple determination because laser (beam homogeneity) timing plays a significant role in the apparent intensity patterns of the mass spectra (see Fig. 3). The relative intensities of the cluster features for 118 nm ionization are generally independent of laser intensity (from 24 mJ/pulse to 3 mJ/pulse at 355 nm), if fragmentation by residual 355 nm radiation is considered.

B. Fragmentation mechanisms for 193 and 355 nm ionization

Consider first ionization by 193 nm radiation. Based on Fig. 1, one can see that 193 nm light at ca. 1.8 mJ/pulse, focused to 0.1×1.0 mm (ca. 2×10^8 W/cm² intensity), generates extreme fragmentation such that the prominent species detected are Zr, ZrO, and Zr_2O_3 . This fragmentation pattern must arise from many (>4) absorbed photons for each cluster. At ca. 1 mJ/pulse of 193 nm laser radiation, the smaller clusters ($m < 5$) are observed with reduced intensity probably because they require a greater number of photons to ionize, and with the reduced energy/pulse (1 versus 2 mJ/pulse), the cluster fragmentation is not so extreme. [Note the ZrO/ Zr_2O_3 ratio in Figs. 1(a) and 1(b).] The “Gaussian-shaped” cluster ion distribution is typical of a fragmentation pattern.¹² Assuming that the neutral cluster distribution consists mainly of the two series of clusters Zr_mO_{2m} and Zr_mO_{2m+1} , in the range of laser energy/pulse 0.5 to 1.0 mJ/pulse, one can suggest that the fragmentation is of the form



A Zr atom is not fragmented if the laser energy is below about 0.8 mJ/pulse because Zr^+ , ZrO^+ , and $Zr_mO_{2m-1}^+$ ($m < 5$) clusters are not observed. At low enough laser energy/pulse (≤ 0.3 mJ/pulse) only $Zr_mO_{2m}^+$ ($m \geq 5$) clusters are observed. This evolving distribution of cluster ions arises because small, more abundant clusters have high ionization energies, and larger, lower ionization energy clusters are not abundant (under these growth conditions). Smaller clusters have lower densities of states, which also reduce the overall cross section for ionization. Thus, we suggest that cluster fragmentation caused by (multiphoton) ionization processes, if it is not extreme, is local such that, for example, $Zr_5O_{10} \xrightarrow[193 \text{ nm}]{} Zr_5O_9 + O$ and $Zr_5O_{11} \xrightarrow[193 \text{ nm}]{} Zr_5O_9 + 2O$. $Zr_4O_{7,8,9}$ are not observed in this instance because $Zr_4O_{8,9}$ are not directly ionized at this photon arrival rate and because $Zr_5O_{10,11}$ do not lose a ZrO, ZrO_2 , ZrO_3 or ZrO_4 in their fragmentation processes.

One can estimate the dissociation probability for $Zr_6O_{12}^+ \xrightarrow[193 \text{ nm}]{} Zr_5O_{10}^+ + ZrO_2$ by using RRK theory and rate equations

$$k(E) = \nu(1 - E_0/E^*)^{s-1}, \quad (1)$$

$$N_f = N_0(1 - e^{-kt}). \quad (2)$$

E_0 is the dissociation energy for the above reaction, and it is assumed to be the same as the dissociation energy of the neutral clusters obtained by DFT calculations at the BPW91/LANL2DZ level²⁴ using the GAUSSIAN 98 program.²⁵ N_0 and N_f are the initial number of cluster ions and the number of fragment ions, respectively. ν is the vibrational frequency of the reaction dissociation coordinate and has a value of $\nu = 10^{13}$ (s⁻¹). s is the number of oscillators in the cluster. Assuming three photons of 193 nm radiation are absorbed, $E^* = 13.67$ eV is the excess energy in the cluster $Zr_6O_{12}^+$ calculated from $E^* = (\text{internal energy in clusters}) + 3 \times 6.4 \text{ eV} - 8.41 \text{ eV}$ (adiabatic ionization energy).¹² The internal energy in the cluster = 2.88 eV due to vibration at an assumed temperature of ca. 500 K.¹² Thus, according to Ref. 12, $k = 1.5 \text{ s}^{-1}$. A value of $t = 1.5 \times 10^{-6}$ s is taken for the residence time of the cluster ion in the ion source region of the TOFMS, and from Eq. (2) a maximum of 14% of the $Zr_6O_{12}^+$ clusters will dissociate to $Zr_5O_{10}^+$ following absorption of three photons by $Zr_6O_{12}^+$. Thus, one can expect only mild fragmentation from Zr_mO_{2m} to $Zr_{m-1}O_{2m-2}$ or from Zr_mO_{2m+1} to $Zr_{m-1}O_{2m-1}$, in general, at relatively high ionization laser energy/pulse.

Consider next the fragmentation mechanism for 355 nm radiation ionization of the two neutral cluster series Zr_mO_{2m} and Zr_mO_{2m+1} . Based on the experimental data presented in this report, the number of absorbed photons of 355 nm light per cluster is not known, so a calculation of expected fragmentation is not available. Nonetheless, Fig. 4 demonstrates that, again, the fragmentation is local (e.g., $Zr_2O_4 \xrightarrow{355 \text{ nm}} Zr_2O_3^+ + O$, $Zr_2O_5 \xrightarrow{355 \text{ nm}} Zr_2O_3^+ + 2O$, and $Zr_3O_6 \xrightarrow{355 \text{ nm}} Zr_2O_4^+ + ZrO_2$) because the $Zr_mO_{2m,2m+1}^+$ mass spectral features are linewidth limited by the laser pulse duration. If fragmentation occurs with loss of a Zr_x ($x = 1, \dots$) species, these features would be broad unless the fragmentation time were less than 1 ns. This fast rate would not be possible unless a cluster were to absorb 10 or more photons of 355 nm light. Since the intensity of 355 nm light is low (< 24 mJ/pulse at 10 ns duration and $0.5 \text{ cm}^2 - 5 \times 10^6$ W/cm²), one does not expect more than three or four photons at 355 nm to be absorbed by a cluster. Thus, again, the most likely fragmentation mechanism for 355 nm ionization is loss of one or two O atoms from a cluster.

Both 355 and 193 nm ionization/fragmentation of these clusters apparently causes the strongest bond (ZrO–183 kcal/mol, O_2 –119 kcal/mol, Zr_2 –<100 kcal/mol) in the cluster to break, clearly the reaction pathway for other fragmentations includes a significant activation energy.

Now consider the possibility of fragmentation by a single 118 nm (10.5 eV) photon. Although the 10 ns linewidth for the 118 nm ionized $Zr_mO_{2m,2m+1}$ cluster series, along with the previously discussed calculations, strongly suggest that this single photon ionization process does not cause neutral cluster fragmentation on a time scale slower than ~1 ns, faster fragmentation is still a logical possibility. One can estimate the 118 nm laser energy/pulse at roughly $0.5 \mu\text{J/pulse}$ which corresponds to ca. 10^{11} photons/pulse.

TABLE I. Vertical and adiabatic ionization energies (eV) of the optimized structure of ZrO and ZrO₂ clusters calculated at BPW91/LANL2DZ level.

| | Vertical ionization energy | Adiabatic ionization energy |
|------------------|----------------------------|-----------------------------|
| ZrO | 6.23 | 6.19 |
| ZrO ₂ | 9.05 | 8.99 |

Using Eq. (1) with the previously employed parameters and 10.5 eV energy for the single absorbed, we obtain $k = 1.1 \times 10^{-32} \text{ s}^{-1}$. This yields a 0% probability of cluster fragmentation of the form $\text{Zr}_m\text{O}_{2m} \rightarrow_{118 \text{ nm}} \text{Zr}_{m-1}\text{O}_{2m-2}^+ + \text{ZrO}_2$.

One can also perform DFT calculations at the BPW91/LANL2DZ level on ZrO, ZrO₂, ZrO⁺, and ZrO₂⁺ to calculate the dissociation energy for the reaction $\text{ZrO}_2^+ \rightarrow_{118 \text{ nm}} \text{ZrO}^+ + \text{O}$. Table I gives the calculated values for the vertical and adiabatic ionization energies for the most stable cluster structures of these neutrals. Ionization energies of ZrO and ZrO₂ clusters have been estimated by electron impact studies to be ca. 6 eV and ca. 9 eV, respectively.²⁶ The calculated vertical values are in quite good agreement with those experimental estimates. The $\text{ZrO}_2^+ \rightarrow \text{ZrO}^+ + \text{O}$ minimum dissociation energy is calculated at 4.4 eV. E^* for 118 nm single photon ionization is $E^* = 10.5 \text{ eV (118 nm photon)} + 2.88 \text{ eV (internal energy)} - 8.99 \text{ eV (adiabatic ionization energy for ZrO}_2) = 4.4 \text{ eV}$. Thus, both E^* and E_{diss} are ca. 4.4 eV and roughly equal. The time for such a dissociation is certainly not less than 1 ns as required for the process to be consistent with the experimental linewidth of the mass spectral features generated by 118 nm ionization. Larger clusters would dissociate even more slowly based on densities of states estimates. Thus, one can conclude that 118 nm radiation used for Zr_mO_{2m} and $\text{Zr}_m\text{O}_{2m+1}$ ionization does not fragment these clusters within the experimental time scale.

The Zr₅O₁₀ cluster appears to have a special stability in the 193 nm derived mass spectrum, as can be seen in Figs. 1 and 7 and as reported in Ref. 12. One can also make this argument based on some of the 118 nm ionization data (Fig. 3), as well as the previously reported DFT calculations.¹² The main difference between the 118 nm and 193 nm derived mass spectral data is that clusters with $m < 5$ have too high an ionization energy and/or too low a density of states for the low energy/pulse ($\leq 0.5 \text{ mJ/pulse}$, Fig. 1) 193 nm studies to generate any ions in this cluster size regime. Zr₅O₁₀ is indeed more intense than Zr₆O₁₂ and Zr₄O₈ under some conditions.

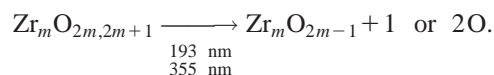
Foltin *et al.* use covariance mapping techniques to identify cluster fragmentation and cluster growth dominated mass spectra. They found that, at high 193 nm laser intensity, fragmentation dominates the mass spectra (the $\text{Zr}_m\text{O}_{2m-1}^+$ series is observed), but at lower laser intensity, the $\text{Zr}_m\text{O}_{2m}^+$, $m \geq 5$ cluster ion series appears, and the covariance map for $\text{Zr}_m\text{O}_{2m-1}^+$ clusters indicates that this latter pattern is due to neutral cluster growth. They did, however, attribute the loss of small cluster ($m < 5$) signals to rapid cluster growth and not high ionization energy/low density of states for $\text{Zr}_m\text{O}_{2m,2m+1}$, $m < 5$. They correctly identify the Zr₅O₁₀ neu-

tral cluster as especially stable based on mass spectral peak intensities and DFT calculations.

V. CONCLUSIONS

The major result of this study is to show that high energy, single photon (10.5 eV, 118 nm), low intensity (10^{11} photons/pulse) photoionization of transition metal oxide neutral clusters (zirconium oxide, Zr_mO_n) can be employed to determine the neutral cluster distribution in the gas phase. Even though one cannot, at present, select individual clusters for study, as one can do with ionic clusters, one can know the neutral cluster relative populations. This information can then be used to study the reactivity and chemistry of the neutral clusters.

The neutral cluster distribution for zirconium oxide clusters consists mainly of two series of clusters, Zr_mO_{2m} and $\text{Zr}_m\text{O}_{2m+1}$. Multiphoton ionization of clusters with 193 and 355 nm laser radiation at moderate energy/pulse and focus (intensity, ca. $1 \times 10^7 \text{ W/cm}^2$, $\sim 1 \text{ mJ/pulse}$) generates fragmentation along with neutral cluster ionization. One can argue that the fragmentation is mostly, if not entirely, local in the sense that



Mass spectral features generated by a tightly focused ($\leq 50 \mu\text{m}$), 118 nm ionization laser are very sharp and their linewidths are governed by the duration of the laser pulse. Such linewidths are the hallmark of nonfragmenting ionization of neutral clusters. The average full width for these features at half-maximum is ca. 10 ns, but individual laser pulses can generate widths as small as a few ns or less due to the laser mode structure.

At low laser intensity for the multiphoton ionization process, cluster ions with $m < 5$ are not observed due to higher cluster ionization energies and lower cluster density of states for the small clusters. These small clusters are also not generated by larger cluster fragmentation at low laser intensities.

We are now in the process of studying the reactions of these neutral clusters with small gas phase molecules.

ACKNOWLEDGMENT

We thank the U.S. DOE Basic Energy Sciences for support of this work.

¹G. Ertl and H. J. Freund, *Phys. Today* **52**, 32 (1993).

²M. Fox and M. T. Dulay, *Chem. Rev.* **93**, 341 (1993).

³A. L. Linsebigler, G. Lu, and J. T. Yates, Jr., *Chem. Rev.* **95**, 735 (1995).

⁴J. P. Donn, H. G. Stenger, and I. E. Wachs, *Catal. Today* **51**, 301 (1999).

⁵X.-C. Guo and R. J. Madix, *Acc. Chem. Res.* **36**, 471 (2003).

⁶E. L. Muetterties, T. N. Robin, E. Brand, C. F. Brucker, and W. Pretzer, *Chem. Rev. (Washington, D.C.)* **79**, 91 (1979).

⁷E. L. Muetterties, *Science* **196**, 839 (1977).

⁸E. F. Fialko, A. V. Kikhtenko, V. B. Goncharov, and K. I. Zamaraev, *J. Phys. Chem. B* **101**, 5772 (1997).

⁹K. A. Zemski, D. R. Justes, and A. W. Castelman, Jr., *J. Phys. Chem. B* **106**, 6136 (2002).

¹⁰P. A. Hackett, S. A. Mitchell, D. M. Rayner, and B. Simard, "Progress toward a molecular surface science: Dative interactions in chemistry and metal centers as revealed by spectroscopic, kinetic, and dynamical stud-

- ies," in *Metal-Ligand Interactions*, edited by R. Russo and D. R. Salahub (Kluwer, Amsterdam, 1996), p. 289.
- ¹¹M. Foltin, G. J. Stueber, and E. R. Bernstein, *J. Chem. Phys.* **111**, 9577 (1999).
- ¹²M. Foltin, G. J. Stueber, and E. R. Bernstein, *J. Chem. Phys.* **114**, 8971 (2001).
- ¹³D. N. Shin, Y. Matsuda, and E. R. Bernstein, *J. Chem. Phys.* **120**, 4150 (2004) (this issue); **120**, 4157 (2004) (this issue); Y. Matsuda, D. N. Shin, and E. R. Bernstein, *ibid.* **120**, 4165 (2004) (this issue); Y. Matsuda and E. R. Bernstein, *J. Chem. Phys.* (to be published).
- ¹⁴X.-C. Guo and R. J. Madix, *Acc. Chem. Res.* **36**, 471 (2003); X.-C. Guo and R. J. Madix, *J. Phys. Chem. B* **107**, 3105 (2003).
- ¹⁵G. von Helden, D. van Heijnsbergen, and G. Meijer, *J. Phys. Chem. A* **107**, 1671 (2003).
- ¹⁶O. C. Thomas, S. J. Xu, T. P. Lippa, and K. H. Bowen, *J. Cluster Sci.* **10**, 525 (1999).
- ¹⁷H.-J. Zhai and L.-S. Wang, *J. Chem. Phys.* **117**, 7882 (2002).
- ¹⁸A. Pramann, K. Koyasu, A. Nakajima, and K. Kaya, *J. Phys. Chem. A* **106**, 4891 (2002).
- ¹⁹D. J. Brugh, R. D. Suenram, and W. J. Stevens, *J. Chem. Phys.* **111**, 3526 (1999).
- ²⁰R. D. Suenram, F. J. Lovas, G. T. Fraser, and K. Matsumura, *J. Chem. Phys.* **92**, 4724 (1990).
- ²¹D. R. Justes, R. Mitric, N. A. Moore, V. Bonacic-Koutecky, and A. W. Castleman, Jr., *J. Am. Chem. Soc.* **125**, 6289 (2003).
- ²²K. Kaizu, M. Kohno, S. Suzuki, H. Shiromaru, T. Moriwaki, and Y. Achiba, *J. Chem. Phys.* **106**, 9954 (1997); T. Wakabayashi, T. Momose, and T. Shida, *ibid.* **111**, 6260 (1999).
- ²³Y. J. Shi, S. Consta, A. K. Das, B. Mallik, D. Lacey, and R. H. Lipson, *J. Chem. Phys.* **116**, 6990 (2002).
- ²⁴K. Burke, P. J. Perdew, and Y. Yang, in *Electronic Density Functional Theory: Recent Progress and New Directions*, edited by J. F. Dobson, G. Vignance, and P. M. Das (Plenum, New York, 1998); J. P. Perdew, in *Electronic Structure of Solids*, edited by P. Ziesche and H. Eschrig (Akademie-Verlag, Berlin, 1991), p. 11; J. P. Perdew, J. A. Chevary, S. H. Vosko, K. A. Jackson, M. R. Pederson, D. J. Singh, and C. Fiol Hais, *Phys. Rev. B* **46**, 6671 (1992); **48**, 4978 (1993); J. P. Perdew, K. Burke, and Y. Wang, *ibid.* **54**, 16533 (1996); A. D. Becke, *J. Chem. Phys.* **104**, 1040 (1996).
- ²⁵M. J. Frisch, G. W. Trucks, H. B. Schlegel *et al.*, GAUSSIAN 98, Revision A.6, Gaussian, Inc., Pittsburgh, PA, 1998.
- ²⁶E. Murad and D. L. Hildenbrand, *J. Chem. Phys.* **63**, 1133 (1975); E. G. Rauh and R. J. Ackermann, *ibid.* **60**, 1396 (1974); K. A. Gingerich, *ibid.* **49**, 14 (1968); W. A. Chupka, J. Berkowitz, and M. G. Inghram, *ibid.* **26**, 1207 (1957).